Pergamon

Int. J. Heat Mass Transfer. Vol. 37, No. 17, pp. 2675–2686, 1994

0017–9310/94 $7.00 + 0.00

0017–9310(94)E0100–9

Transient two-dimensional radiative and conductive heat transfer in a scattering medium

CHIH-YANG WU and NAI-RUI OU

Department of Mechanical Engineering, National Cheng Kung University, Tainan, Taiwan 701, Republic of China

(*Received* 11 *August* 1993 *and in final form* 11 *March* 1994)

Abstract—This work considers transient radiative and conductive heat transfer in a rectangular, absorbing–emitting and isotropically scattering medium. An integral-equation method and a modified differential approximation are applied to the radiation part of the present problem. Then, the radiation part and the energy equation are solved by numerical methods simultaneously. Comparisons to results published elsewhere for the special cases of steady-state two-dimensional and transient one-dimensional heat transfer are made. The comparisons show that, along with a finite-difference scheme, the integral-equation method generates very accurate results. The influence of aspect ratios, scattering albedos and conduction-to-radiation parameters is investigated.

1. INTRODUCTION

IN A NUMBER of engineering applications it is necessary to analyze radiative and conductive heat transfer in a semi-transparent medium. Examples of such media are glasses, low-density refractories and ceramics. Lists of previous work on combined radiation and conduction heat transfer can be found in a review article [1] and a textbook [2]. Most of the previous work is confined to one-dimensional cases. In recent years, the steady-state multidimensional case has been a subject of increasing interest. The P-N approximation [3], the finite-element method [4] and the rigorous method [5] were applied to examine the interaction of conduction and radiation in a rectangular, absorbing and emitting medium. Previous studies [6–8] and a few references cited therein have taken the scattering effects into account. However, little work considering transient multidimensional radiation and conduction has been reported. Amlin and Korpela [9] applied the P-1 approximation of radiation to study the transient conductive and radiative heat transfer in a rectangular absorbing–emitting medium. Derevyanko and Koltun [10] proposed a combination of the Monte Carlo method and the finite-difference method for calculating the two-dimensional nonsteady radiative–conductive heat transfer. The above work on transient multidimensional problems has not taken scattering into account.

The present work considers transient radiative and conductive heat transfer in a rectangular, absorbing–emitting and isotropically scattering medium. The analysis of interactive radiation and conduction is made complicated by the nonlinear and nonlocal character of the radiation phenomenon. For the present scattering case, the solution of the radiation part in terms of the temperature cannot be found analytically. Therefore, an exact integral equation method [11] and a modified differential approximation [12–14] are applied to the radiation part of the present problem. The integral terms of the two formulations are obtained by the quadrature methods, while a finite-difference scheme is applied to the differential terms. The objectives of the present work are to demonstrate the heat transfer characteristics of the present transient two-dimensional combined-mode problem and to illustrate the application of the two methods to the radiation part of the problem.

2. ANALYSIS

2.1. *Exact integral formulation*

The simultaneous transport of energy by conduction and radiation in a rectangular semi-transparent medium may be described in terms of the geometry and an associated coordinate system shown in Fig. 1. The present work assumes that the medium absorbs, emits and isotropically scatters radiation, the thermal and radiation properties are constant, and the boundary surfaces are non reflecting. The medium, which is initially at a uniform temperature T_0, is externally heated or cooled from boundaries at fixed temperatures. Here, the boundary surface at $z = 0$ is kept at temperature T_1, while the remaining three boundaries at $z = c, y = 0$ and b are kept at temperature T_2.

The energy equation in terms of the dimensionless temperature θ and radiative heat flux $\mathbf{Q}^r$ is

$$\nabla \cdot \nabla\theta(Y,Z,\xi) - \frac{1}{N}\nabla \cdot \mathbf{Q}^r(Y,Z,\xi) = \frac{\partial\theta(Y,Z,\xi)}{\partial\xi} \quad \text{for } 0 \leqslant Y \leqslant B, 0 \leqslant Z \leqslant C \quad (1)$$

where the operator ∇ is defined for two-dimensional cases as

NOMENCLATURE

b thickness in the y direction
B optical thickness in the y direction, Fig. 1
c thickness in the z direction
C optical thickness in the z direction, Fig. 1
C_p heat capacity
G_m solid-angle-integrated intensity contributed by the medium
G_w solid-angle-integrated intensity contributed by the boundary
I dimensionless radiation intensity
I_b dimensionless total blackbody radiation intensity
$\mathbf{j}$ unit vector in the y direction
k thermal conductivity
$\mathbf{k}$ unit vector in the z direction
n refractive index of the medium
N conduction-to-radiation parameter, equation (2b)
N_i total number of quadrature or grid points in the y direction
N_j total number of quadrature or grid points in the z direction
p_k optical distance, $k = 0, 1, \ldots, 4$, equations (10) and (18)
$\mathbf{Q}$ dimensionless heat flux
S dimensionless source function
S_m generalized exponential integral function, equation (11)
t time
T_r reference temperature
T_0 temperature at $t = 0$
T_1 temperature at $z = 0$
T_2 temperature at $y = 0$, b, and $z = c$
y, z coordinates
Y, Z optical coordinates, Fig. 1.

Greek symbols

α aspect ratio
β extinction coefficient
$\Delta\xi$ increment of dimensionless time
ΔY optical distance between grid points in the y direction
ΔZ optical distance between grid points in the z direction
θ dimensionless temperature
θ_0 dimensionless temperature at $\xi = 0$
θ_1 dimensionless temperature at $Z = 0$
θ_2 dimensionless temperature at $Y = 0$, B, and $Z = C$
μ directional cosine of the polar angle, Fig. 1
ξ dimensionless time
ρ density
$\bar{\sigma}$ Stefan–Boltzmann constant
φ azimuthal angle, Fig. 1
ω scattering albedo.

Subscripts and superscripts

i ith grid point in the y direction
j jth grid point in the z direction
n nth time step
r radiation
y y direction
z z direction.

Other symbol

∇ operator, equation (2a).

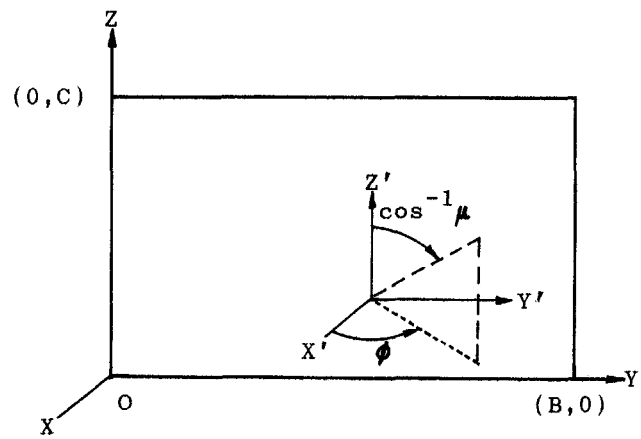

FIG. 1. Geometry and coordinates.

$$\nabla = \frac{\partial}{\partial Y}\mathbf{j} + \frac{\partial}{\partial Z}\mathbf{k} \tag{2a}$$

Y and Z are the optical coordinates defined as the products of the geometrical coordinates and the extinction coefficient β, $\xi = k\beta^2 t/\rho C_p$ is the dimensionless time, $B = b\beta$, $C = c\beta$, and the conduction-to-radiation parameter is defined as

$$N = \frac{k\beta}{n^2\bar{\sigma}T_r^3} \tag{2b}$$

with k, ρ, and C_p being the thermal conductivity, density, and heat capacity of the medium, respectively, $\bar{\sigma}$ the Stefan–Boltzmann constant, t the time, and T_r a selected reference temperature. Here θ and $\mathbf{Q}^r$ are non-dimensionalized by dividing the temperature and the radiative heat flux, respectively, by T_r and $n^2\bar{\sigma}T_r^4$. The boundary conditions for equation (1) are

$$\theta(Y,0,\xi) = \theta_1 \quad 0 \leqslant Y \leqslant B \tag{3a}$$

$$\theta(Y,C,\xi) = \theta_2 \quad 0 \leqslant Y \leqslant B \tag{3b}$$

$$\theta(0,Z,\xi) = \theta_2 \quad 0 \leqslant Z \leqslant C \tag{3c}$$

$$\theta(B,Z,\xi) = \theta_2 \quad 0 \leqslant Z \leqslant C. \tag{3d}$$

The initial condition is

$$\theta(Y,Z,0) = \theta_0, \quad \text{in } 0 \leqslant Y \leqslant B, 0 \leqslant Z \leqslant C. \tag{4}$$

In the present work, we take the reference temperature and initial temperature to be equal to T_1 and T_2, respectively. Hence, $\theta_1 = 1$ and $\theta_0 = \theta_2$.

The transport equation of radiation and boundary conditions to this problem can be expressed as

$$\sqrt{1-\mu^2}\sin\varphi\frac{\partial I(Y,Z,\mu,\varphi)}{\partial Y} + \mu\frac{\partial I(Y,Z,\mu,\varphi)}{\partial Z} + I(Y,Z,\mu,\varphi) = S(Y,Z)$$

$$\text{for } 0 \leqslant Y \leqslant B, 0 \leqslant Z \leqslant C, -1 \leqslant \mu \leqslant 1, 0 \leqslant \varphi \leqslant 2\pi \tag{5}$$

and

$$I(Y,0,\mu,\varphi) = I_b(\theta_1) \quad 0 \leqslant Y \leqslant B, 0 \leqslant \mu \leqslant 1, 0 \leqslant \varphi \leqslant 2\pi \tag{6a}$$

$$I(Y,C,\mu,\varphi) = I_b(\theta_2) \quad 0 \leqslant Y \leqslant B, -1 \leqslant \mu \leqslant 0, 0 \leqslant \varphi \leqslant 2\pi \tag{6b}$$

$$I(0,Z,\mu,\varphi) = I_b(\theta_2) \quad 0 \leqslant Z \leqslant C, -1 \leqslant \mu \leqslant 1, 0 \leqslant \varphi \leqslant \pi \tag{6c}$$

$$I(B,Z,\mu,\varphi) = I_b(\theta_2) \quad 0 \leqslant Z \leqslant C, -1 \leqslant \mu \leqslant 1, \pi \leqslant \varphi \leqslant 2\pi \tag{6d}$$

where μ is the directional cosine of the polar angle, φ the azimuthal angle, I the dimensionless radiation intensity, I_b the dimensionless blackbody radiation intensity defined as

$$I_b(\theta) = \theta^4 \tag{7}$$

and S is the dimensionless source function defined as

$$S(Y,Z) = (1-\omega)I_b(\theta) + \frac{\omega}{4\pi}\int_{\mu=-1}^{1}\int_{\varphi=0}^{2\pi} I(Y,Z,\mu,\varphi)\,d\varphi\,d\mu \tag{8}$$

with ω being the scattering albedo. Here, I and S are non-dimensionalized by dividing the intensity and the source function by $n^2\bar{\sigma}T_r^4/\pi$, respectively.

Finding the formal solution of intensity, substituting the resulting equation into equation (8) and transforming the resulting integrals over solid angle into surface and volume integrals [11], one can obtain the exact integral expression for the source function as

$$S(Y,Z) = (1-\omega)I_b(\theta) + \omega I_b(\theta_2) + \frac{\omega}{4}\int_0^B [I_b(\theta_1) - I_b(\theta_2)]\frac{S_2(p_1)}{p_1^2}Z\,dY' + \frac{\omega}{4}\int_0^C\int_0^B [S(Y',Z') - I_b(\theta_2)]\frac{S_1(p_0)}{p_0}dY'\,dZ' \tag{9}$$

where

$$p_0 = [(Y-Y')^2 + (Z-Z')^2]^{1/2} \tag{10a}$$

$$p_1 = [(Y-Y')^2 + Z^2]^{1/2} \tag{10b}$$

and S_m is a generalized exponential integral function defined by

$$S_m(p) = \frac{2}{\pi}\int_1^\infty \frac{\exp(-p\tau)}{\tau^m(\tau^2-1)^{1/2}}d\tau \quad m = 1,2,3,\ldots. \tag{11}$$

Using a similar procedure, one can also obtain the exact expressions for the y component and the z component of radiative flux

$$Q_y^r(Y,Z) = \int_0^C\int_0^B [S(Y',Z') - I_b(\theta_2)] \times \frac{S_2(p_0)}{p_0^2}(Y-Y')\,dY'\,dZ' + Z\int_0^B [I_b(\theta_1) - I_b(\theta_2)] \times \frac{S_3(p_1)}{p_1^3}(Y-Y')\,dY' \tag{12}$$

$$Q_z^r(Y,Z) = \int_0^C\int_0^B [S(Y',Z') - I_b(\theta_2)] \times \frac{S_2(p_0)}{p_0^2}(Z-Z')\,dY'\,dZ' + Z^2\int_0^B [I_b(\theta_1) - I_b(\theta_2)] \times \frac{S_3(p_1)}{p_1^3}dY' \tag{13}$$

respectively.

The system of equations to be solved is equations (1) and (9). The two equations are coupled by the divergence of radiative flux in equation (1) and the

emission term in equation (9). The divergence of radiative flux may be expressed as

$$\nabla\cdot\mathbf{Q}^{r}(Y,Z)=(1-\omega)\left\{4[I_b(\theta)-I_b(\theta_2)]-\int_0^B[I_b(\theta_1)-I_b(\theta_2)]\frac{S_2(p_1)}{p_1^2}Z\,dY'-\int_0^C\int_0^B[S(Y',Z')-I_b(\theta_2)]\frac{S_1(p_0)}{p_0}dY'\,dZ'\right\}. \quad (14)$$

When $\omega=0$, $S=\theta^4$ and so we do not need to solve equation (9).

2.2. *Modified differential approximation (MDA)*

For the present problem, the MDA for the radiation part can be expressed as the differential equation

$$\nabla^2 G_m=4(1-\omega)I_b(\theta)+3(1-\omega)(G_m+G_w)-3G_w \quad \text{for } 0\leqslant Y\leqslant B,\ 0\leqslant Z\leqslant C \quad (15)$$

with the boundary conditions

$$2(\partial G_m/\partial Z)/3=G_m \quad \text{at } Z=0 \quad (16a)$$

$$2(\partial G_m/\partial Z)/3=-G_m \quad \text{at } Z=C \quad (16b)$$

$$2(\partial G_m/\partial Y)/3=G_m \quad \text{at } Y=0 \quad (16c)$$

$$2(\partial G_m/\partial Y)/3=-G_m \quad \text{at } Y=B \quad (16d)$$

where G_m and G_w are the solid-angle-integrated intensity contributed respectively by the medium and the boundary. For the present problem G_w may be expressed in dimensionless form as

$$G_w(Y,Z)=Z\int_0^B I_b(\theta_1)\frac{S_2(p_1)}{p_1^2}dY'+(B-Y)\int_0^C I_b(\theta_2)\frac{S_2(p_2)}{p_2^2}dZ'+(C-Z)\int_0^B I_b(\theta_2)\frac{S_2(p_3)}{p_3^2}dY'+Y\int_0^C I_b(\theta_2)\frac{S_2(p_4)}{p_4^2}dZ' \quad (17)$$

where

$$p_2=[(Y-B)^2+(Z-Z')^2]^{1/2} \quad (18a)$$

$$p_3=[(Y-Y')^2+(Z-C)^2]^{1/2} \quad (18b)$$

$$p_4=[Y^2+(Z-Z')^2]^{1/2}. \quad (18c)$$

The divergence of radiative flux in equation (1) can be expressed in terms of G_m and G_w by

$$\nabla\cdot\mathbf{Q}^{r}=4(1-\omega)I_b(\theta)+(\omega-1)(G_m+G_w). \quad (19)$$

The radiative flux in terms of G_m can be expressed as

$$Q_y^r(Y,Z)=-\frac{1}{3}\frac{\partial G_m}{\partial Y}+Z\int_0^B I_b(\theta_1)\frac{S_3(p_1)}{p_1^3}(Y-Y')\,dY'+(Y-B)^2\int_0^C I_b(\theta_2)\frac{S_3(p_2)}{p_2^3}dZ'+(Z-C)\int_0^B I_b(\theta_2)\frac{S_3(p_3)}{p_3^3}(Y-Y')\,dY'+Y^2\int_0^C I_b(\theta_2)\frac{S_3(p_4)}{p_4^3}dZ' \quad (20a)$$

$$Q_z^r(Y,Z)=-\frac{1}{3}\frac{\partial G_m}{\partial Z}+Z^2\int_0^B I_b(\theta_1)\frac{S_3(p_1)}{p_1^3}dY'+(Y-B)\int_0^C I_b(\theta_2)\frac{S_3(p_2)}{p_2^3}(Z-Z')\,dZ'+(Z-C)^2\int_0^B I_b(\theta_2)\frac{S_3(p_3)}{p_3^3}dY'+Y\int_0^C I_b(\theta_2)\frac{S_3(p_4)}{p_4^3}(Z-Z')\,dZ'. \quad (20b)$$

2.3. *Numerical procedure*

For the exact formulation, the system of equations to be solved is equations (1) and (9) for the two unknowns θ and S, respectively. Crosbie and Schrenker [11] have obtained highly accurate solutions for the integral equation of radiative transfer in a rectangular medium by using the Labatto's quadrature and singularity-subtraction technique. When the Gaussian quadrature is used, results of the same degree of accuracy can be obtained by fewer quadrature points [11]. However, solutions at the boundary of the medium cannot be obtained by the Gaussian quadrature directly. Here, we adopt either of the quadrature methods to solve the radiation part the present problem.

The conduction part is solved by a finite-difference scheme. Using a central difference approximation for the second-order space derivatives of θ at each interior grid point yields

$$(\nabla\cdot\nabla\theta)_{i,j}^n=\frac{2[\theta_{i+1,j}^n-\theta_{i,j}^n]}{\Delta Y_i(\Delta Y_{i+1}+\Delta Y_{i-1})}-\frac{2[\theta_{i,j}^n-\theta_{i-1,j}^n]}{\Delta Y_{i-1}(\Delta Y_{i+1}+\Delta Y_{i-1})}+\frac{2[\theta_{i,j+1}^n-\theta_{i,j}^n]}{\Delta Z_j(\Delta Z_{j+1}+\Delta Z_{j-1})}-\frac{2[\theta_{i,j}^n-\theta_{i,j-1}^n]}{\Delta Z_{j-1}(\Delta Z_{j+1}+\Delta Z_{j-1})}$$
$$i=2,3,\ldots,N_i-1,\quad j=2,3,\ldots,N_j-1,\quad n=0,1,2,\ldots \quad (21)$$

where the subscripts i and j represent the spatial location in the y and z direction, respectively, the superscript n represents the nth time step, $\Delta Y_i = Y_{i+1} - Y_i$, and $\Delta Z_j = Z_{j+1} - Z_j$. Using the Crank–Nicolson scheme to approximate the step-wise marching in time away from the given initial condition, the finite-difference approximation of equation (1) becomes

$$\theta_{i,j}^{n+1} - \theta_{i,j}^{n} = \frac{\Delta\xi^n}{2}[(\nabla\cdot\nabla\theta)_{i,j}^{n} + (\nabla\cdot\nabla\theta)_{i,j}^{n+1}] - \frac{\Delta\xi^n}{N}(\nabla\cdot\mathbf{Q}^r)_{i,j}^{n} \quad (22)$$

where $\Delta\xi^n = \xi^{n+1} - \xi^n$ is a variable increment of time. At the beginning of time marching, to treat an abrupt change in boundary temperature a small $\Delta\xi^n$ is chosen. After $|\partial\theta/\partial\xi|$ becomes small, a larger $\Delta\xi^n$ is used.

Equations (1) and (9) are solved using different grid points. Hence to solve equations (1) and (9) simultaneously, a bicubic spline two-dimensional interpolation is used.

Gauss–Sidel iteration is used to solve equation (22). The temperature and the source function are iterated at a given time until the current iteration and the previous iteration meet the absolute convergence criterion that

$$|\theta^{(\text{current})}(Y,Z,\xi) - \theta^{(\text{previous})}(Y,Z,\xi)| < 10^{-8} \quad (23)$$

at each grid point. After finding the temperature at each grid point at the given time step, the scheme calculates the radiative flux at the given time step, and then repeats the same calculation procedure at the next time step. This recursive procedure is continued until steady state is reached. The criterion for steady state is generally $|\partial\theta/\partial\xi| < 10^{-4}$ at each grid point.

For the MDA, the system of equations to be solved is equations (1) and (15). Since equation (15) is similar to the steady-state version of equation (1), it can be solved by a numerical scheme similar to that used to solve equation (1) at a given time step.

3. RESULTS AND DISCUSSION

Since accurate results for the present transient two-dimensional problem are not available, the results of the present work are benchmarked against the published work of two special cases: the steady-state two-dimensional case of Yuen and Takara [5] and the transient one-dimensional case of Lii and Özisik [15] and Sutton [16].

In the current model, the one-dimensional case corresponds to the special case of $B \to \infty$. In Table 1, the temperature and the radiative heat flux along the z direction at the symmetry plane $Y = B/2$ of a wide rectangular medium are compared against those of the one-dimensional case. The present results are obtained by the Labatto's quadrature with $N_j = 15$. As shown in Table 1, the results of the wide rectangular medium are in good agreement with those of Sutton's one-dimensional work [16]. This agreement supports the accuracy of the present computation for transient cases. However, two discrepancies are found. The smaller discrepancy between the present results and Sutton's results [16] may be attributed to the y-direction heat transfer of the present two-dimensional model, whereas the discrepancy between Lii and Özisik's results [15] and the others has been addressed in Sutton's work [16].

The results for the steady-state problem in a rectangular medium are obtained by setting $\theta_1 = 1$ at the bottom surface and $\theta_2 = 0.5$ at the other surfaces. Tables 2 and 3 show the temperature and the heat-flux distributions at the symmetry plane $Y = B/2$ and the center plane $Z = C/2$, respectively. Those results shown are obtained by using 11×11 elements in ref. [5] and using 11×11 and 21×21 Gaussian quadrature points in the present, more general model. Each of Tables 2 and 3 includes three sets of results, (a), (b) and (c), for $B = C = 0.1$, 1 and 5, respectively. The discrepancy between the results obtained by the present work and those obtained by Yuen and Takara [5] increases as the optical size of the medium increases, as shown in Tables 2 and 3. The discrepancy is quite small for the conduction-dominated case of $N = 4$. Hence, the discrepancy is due to the solutions of the integral equation of radiative transfer.

To illustrate further the accuracy of the numerical results, the wall heat flux at each boundary and the overall energy balance for a square medium with $B = C = 1$ are presented in Table 4. For various values of N overall energy balance is achieved within

Table 1. Comparative results of the transient temperature distributions of a wide rectangular medium ($B = 5.0$, $C = 1.0$) and a planar medium ($C = 1.0$) with $\omega = 0.5$, $N = 0.4$, $\theta_0 = 0$, $\theta_1 = 1.0$ and $\theta_2 = 0.0$, at $\xi = 0.05$

	Ref.	$Z/C = 0.25$	0.50	0.75
Temperature	[15]	0.4617	0.1474	0.0277
	[16]	0.4888	0.1778	0.0591
	This work	0.4864	0.1775	0.0589
Radiative flux	[15]	1.6436	1.2529	0.9746
	[16]	1.9304	1.3305	0.8332
	This work	1.9178	1.3310	0.8391

Table 2(a). Comparative results of $\theta(B/2, Z)$ and $Q_z(B/2, Z)$ for square media with $B = C = 0.1$ and various values of N by three schemes

N	No. of grids or elements	$Z/C =$	1.0	0.7	0.5	0.3	0.0
4.0	11×11 [5]	$\theta =$	0.500	0.560	0.625	0.733	1.000
		$Q_z =$	7.473	10.795	17.369	28.074	41.144
	11×11 (this work)	$\theta =$	0.500	0.560	0.625	0.733	1.000
		$Q_z =$	7.474	10.795	17.369	28.075	41.144
	21×21 (this work)	$\theta =$	0.500	0.560	0.626	0.733	1.000
		$Q_z =$	7.476	10.795	17.369	28.075	41.144
0.4	11×11 [5]	$\theta =$	0.500	0.561	0.626	0.733	1.000
		$Q_z =$	1.100	1.542	2.305	3.503	4.932
	11×11 (this work)	$\theta =$	0.500	0.567	0.633	0.733	1.000
		$Q_z =$	1.100	1.542	2.304	3.504	4.932
	21×21 (this work)	$\theta =$	0.500	0.563	0.630	0.733	1.000
		$Q_z =$	1.100	1.542	2.304	3.504	4.392
0.04	11×11 [5]	$\theta =$	0.500	0.567	0.633	0.738	1.000
		$Q_z =$	0.462	0.616	0.798	1.046	1.311
	11×11 (this work)	$\theta =$	0.500	0.568	0.634	0.738	1.000
		$Q_z =$	0.462	0.616	0.798	1.033	1.310
	21×21 (this work)	$\theta =$	0.500	0.568	0.634	0.738	1.000
		$Q_z =$	0.462	0.616	0.798	1.033	1.310
0.004	11×11 [5]	$\theta =$	0.500	0.615	0.680	0.766	1.000
		$Q_z =$	0.398	0.524	0.648	0.801	0.949
	11×11 (this work)	$\theta =$	0.500	0.615	0.680	0.766	1.000
		$Q_z =$	0.398	0.524	0.648	0.801	0.949
	21×21 (this work)	$\theta =$	0.500	0.615	0.680	0.766	1.000
		$Q_z =$	0.398	0.525	0.648	0.801	0.950

Table 2(b). Comparative results of $\theta(B/2, Z)$ and $Q_z(B/2, Z)$ for square media with $B = C = 1.0$ and various values of N by three schemes

N	No. of grids or elements	$Z/C =$	1.0	0.7	0.5	0.3	0.0
4.0	11×11 [5]	$\theta =$	0.500	0.564	0.630	0.737	1.000
		$Q_z =$	0.927	1.352	2.112	3.315	4.701
	11×11 (this work)	$\theta =$	0.500	0.564	0.630	0.736	1.000
		$Q_z =$	0.941	1.354	2.100	3.311	4.740
	21×21 (this work)	$\theta =$	0.500	0.560	0.630	0.733	1.000
		$Q_z =$	0.941	1.354	2.102	3.313	4.740
0.4	11×11 [5]	$\theta =$	0.500	0.589	0.661	0.763	1.000
		$Q_z =$	0.289	0.430	0.609	0.860	1.083
	11×11 (this work)	$\theta =$	0.500	0.593	0.663	0.759	1.000
		$Q_z =$	0.304	0.432	0.599	0.854	1.111
	21×21 (this work)	$\theta =$	0.500	0.590	0.663	0.760	1.000
		$Q_z =$	0.304	0.433	0.602	0.855	1.112
0.04	11×11 [5]	$\theta =$	0.500	0.653	0.726	0.807	1.000
		$Q_z =$	0.222	0.344	0.463	0.610	0.780
	11×11 (this work)	$\theta =$	0.500	0.664	0.725	0.791	1.000
		$Q_z =$	0.233	0.340	0.446	0.602	0.759
	21×21 (this work)	$\theta =$	0.500	0.663	0.725	0.791	1.000
		$Q_z =$	0.230	0.341	0.449	0.605	0.755
0.004	11×11 [5]	$\theta =$	0.500	0.685	0.736	0.794	1.000
		$Q_z =$	0.226	0.322	0.423	0.556	0.722
	11×11 (this work)	$\theta =$	0.500	0.684	0.736	0.795	1.000
		$Q_z =$	0.220	0.324	0.424	0.570	0.723
	21×21 (this work)	$\theta =$	0.500	0.684	0.736	0.795	1.000
		$Q_z =$	0.220	0.323	0.424	0.564	0.722

Table 2(c). Comparative results of $\theta(B/2, Z)$ and $Q_z(B/2, Z)$ for square media with $B = C = 5.0$ and various values of N by three schemes

N	No. of grids or elements		$Z/C =$	1.0	0.7	0.5	0.3	0.0
4.0	11 × 11	[5]	$\theta =$	0.500	0.567	0.640	0.755	1.000
			$Q_z =$	0.173	0.298	0.514	0.858	1.034
	11 × 11	(this work)	$\theta =$	0.500	0.576	0.648	0.756	1.000
			$Q_z =$	0.210	0.315	0.494	0.812	1.192
	21 × 21	(this work)	$\theta =$	0.500	0.576	0.648	0.756	1.000
			$Q_z =$	0.209	0.311	0.491	0.813	1.205
0.4	11 × 11	[5]	$\theta =$	0.500	0.585	0.689	0.834	1.000
			$Q_z =$	0.039	0.130	0.257	0.408	0.253
	11 × 11	(this work)	$\theta =$	0.500	0.626	0.707	0.802	1.000
			$Q_z =$	0.086	0.136	0.191	0.328	0.459
	21 × 21	(this work)	$\theta =$	0.500	0.626	0.707	0.802	1.000
			$Q_z =$	0.086	0.136	0.195	0.330	0.452
0.04	11 × 11	[5]	$\theta =$	0.500	0.658	0.732	0.814	1.000
			$Q_z =$	0.068	0.111	0.165	0.245	0.388
	11 × 11	(this work)	$\theta =$	0.500	0.655	0.733	0.818	1.000
			$Q_z =$	0.071	0.119	0.160	0.275	0.388
	21 × 21	(this work)	$\theta =$	0.500	0.656	0.733	0.818	1.000
			$Q_z =$	0.071	0.116	0.164	0.275	0.390
0.004	11 × 11	[5]	$\theta =$	0.500	0.665	0.738	0.817	1.000
			$Q_z =$	0.071	0.110	0.161	0.238	0.380
	11 × 11	(this work)	$\theta =$	0.500	0.661	0.737	0.821	1.000
			$Q_z =$	0.069	0.117	0.157	0.269	0.386
	21 × 21	(this work)	$\theta =$	0.500	0.661	0.737	0.821	1.000
			$Q_z =$	0.068	0.115	0.161	0.269	0.386

Table 3(a). Comparative results of $\theta(Y, C/2)$, $Q_z(Y, C/2)$ and $Q_y(Y, C/2)$ for square media with $B = C = 0.1$ and various values of N by three schemes

N	No. of grids or elements		$Y/B =$	0.6	0.8	1.0
4.0	11 × 11	[5]	$\theta =$	0.620	0.577	0.500
			$Q_z =$	16.819	11.800	0.395
			$Q_y =$	4.347	12.619	16.839
	11 × 11	(this work)	$\theta =$	0.620	0.577	0.500
			$Q_z =$	16.819	11.800	0.395
			$Q_y =$	4.347	12.619	16.839
	21 × 21	(this work)	$\theta =$	0.620	0.577	0.500
			$Q_z =$	16.819	11.800	0.395
			$Q_y =$	4.347	12.619	16.839
0.4	11 × 11	[5]	$\theta =$	0.621	0.578	0.500
			$Q_z =$	2.241	1.668	0.395
			$Q_y =$	0.494	1.431	1.919
	11 × 11	(this work)	$\theta =$	0.620	0.578	0.500
			$Q_z =$	2.241	1.669	0.395
			$Q_y =$	0.494	1.431	1.919
	21 × 21	(this work)	$\theta =$	0.620	0.578	0.500
			$Q_z =$	2.241	1.669	0.395
			$Q_y =$	0.494	1.431	1.919
0.04	11 × 11	[5]	$\theta =$	0.628	0.583	0.500
			$Q_z =$	0.783	0.655	0.395
			$Q_y =$	0.109	0.312	0.427
	11 × 11	(this work)	$\theta =$	0.628	0.583	0.500
			$Q_z =$	0.783	0.655	0.395
			$Q_y =$	0.109	0.312	0.426
	21 × 21	(this work)	$\theta =$	0.628	0.583	0.500
			$Q_z =$	0.783	0.655	0.395
			$Q_y =$	0.109	0.312	0.426
0.004	11 × 11	[5]	$\theta =$	0.674	0.620	0.500
			$Q_z =$	0.638	0.554	0.395
			$Q_y =$	0.070	0.200	0.277
	11 × 11	(this work)	$\theta =$	0.674	0.620	0.500
			$Q_z =$	0.638	0.554	0.395
			$Q_y =$	0.071	0.200	0.278
	21 × 21	(this work)	$\theta =$	0.674	0.620	0.500
			$Q_z =$	0.638	0.554	0.395
			$Q_y =$	0.071	0.200	0.278

Table 3(b). Comparative results of $\theta(Y, C/2)$, $Q_x(Y, C/2)$ and $Q_y(Y, C/2)$ for square media with $B = C = 1.0$ and various values of N by three schemes

N	No. of grids or elements		$Y/B =$	0.6	0.8	1.0
4.0	11×11	[5]	$\theta =$	0.624	0.580	0.500
			$Q_x =$	2.050	1.489	0.238
			$Q_y =$	0.491	1.422	1.898
	11×11	(this work)	$\theta =$	0.624	0.580	0.500
			$Q_x =$	2.040	1.485	0.240
			$Q_y =$	0.490	1.425	1.910
	21×21	(this work)	$\theta =$	0.624	0.580	0.500
			$Q_x =$	2.045	1.485	0.240
			$Q_y =$	0.491	1.425	1.905
0.4	11×11	[5]	$\theta =$	0.654	0.603	0.500
			$Q_x =$	0.595	0.478	0.240
			$Q_y =$	0.107	0.305	0.404
	11×11	(this work)	$\theta =$	0.655	0.605	0.500
			$Q_x =$	0.585	0.474	0.240
			$Q_y =$	0.106	0.309	0.414
	21×21	(this work)	$\theta =$	0.654	0.603	0.500
			$Q_x =$	0.590	0.478	0.240
			$Q_y =$	0.106	0.309	0.409
0.04	11×11	[5]	$\theta =$	0.721	0.669	0.500
			$Q_x =$	0.454	0.381	0.245
			$Q_y =$	0.070	0.195	0.250
	11×11	(this work)	$\theta =$	0.720	0.679	0.500
			$Q_x =$	0.438	0.371	0.243
			$Q_y =$	0.069	0.195	0.260
	21×21	(this work)	$\theta =$	0.720	0.679	0.500
			$Q_x =$	0.438	0.371	0.243
			$Q_y =$	0.069	0.195	0.260
0.004	11×11	[5]	$\theta =$	0.733	0.711	0.500
			$Q_x =$	0.416	0.357	0.242
			$Q_y =$	0.059	0.171	0.243
	11×11	(this work)	$\theta =$	0.730	0.710	0.500
			$Q_x =$	0.417	0.357	0.241
			$Q_y =$	0.062	0.172	0.240
	21×21	(this work)	$\theta =$	0.730	0.710	0.500
			$Q_x =$	0.417	0.357	0.241
			$Q_y =$	0.060	0.172	0.240

Table 3(c). Comparative results of $\theta(Y, C/2)$, $Q_z(Y, C/2)$ and $Q_y(Y, C/2)$ for square media with $B = C = 5.0$ and various values of N by three schemes

N	No. of grids or elements	$Y/B =$	0.6	0.8	1.0
4.0	11×11 [5]	$\theta =$	0.634	0.586	0.500
		$Q_z =$	0.496	0.344	0.039
		$Q_y =$	0.125	0.344	0.418
	11×11 (this work)	$\theta =$	0.642	0.594	0.500
		$Q_z =$	0.474	0.342	0.040
		$Q_y =$	0.126	0.366	0.478
	21×21 (this work)	$\theta =$	0.642	0.595	0.500
		$Q_z =$	0.478	0.340	0.040
		$Q_y =$	0.125	0.363	0.478
0.4	11×11 [5]	$\theta =$	0.681	0.614	0.500
		$Q_z =$	0.245	0.164	0.048
		$Q_y =$	0.059	0.137	0.113
	11×11 (this work)	$\theta =$	0.702	0.655	0.500
		$Q_z =$	0.183	0.141	0.048
		$Q_y =$	0.050	0.145	0.190
	21×21 (this work)	$\theta =$	0.702	0.654	0.500
		$Q_z =$	0.189	0.144	0.048
		$Q_y =$	0.046	0.135	0.191
0.04	11×11 [5]	$\theta =$	0.728	0.692	0.500
		$Q_z =$	0.161	0.129	0.061
		$Q_y =$	0.034	0.099	0.149
	11×11 (this work)	$\theta =$	0.727	0.690	0.500
		$Q_z =$	0.154	0.121	0.053
		$Q_y =$	0.041	0.117	0.144
	21×21 (this work)	$\theta =$	0.728	0.690	0.500
		$Q_z =$	0.160	0.126	0.055
		$Q_y =$	0.036	0.118	0.146
0.004	11×11 [5]	$\theta =$	0.734	0.700	0.500
		$Q_z =$	0.158	0.128	0.063
		$Q_y =$	0.032	0.095	0.153
	11×11 (this work)	$\theta =$	0.730	0.695	0.500
		$Q_z =$	0.157	0.119	0.053
		$Q_y =$	0.040	0.113	0.137
	21×21 (this work)	$\theta =$	0.730	0.695	0.500
		$Q_z =$	0.157	0.115	0.056
		$Q_y =$	0.040	0.115	0.138

Table 4. Comparative results of the wall heat flux at each boundary for a square medium with $B = C = 1.0$, $N = 0.4$, $\theta_1 = 1.0$ and $\theta_2 = 0.5$ by three schemes

N		Integral [5]	This work 11×11	This work 21×21
4.0	Bottom wall	3.157	3.339	4.245
	Side wall	2.824	3.027	3.931
	Top wall	0.316	0.324	0.322
	% error	0.54	0.36	0.19
0.4	Bottom wall	0.649	0.639	0.751
	Side wall	0.518	0.529	0.635
	Top wall	0.114	0.121	0.122
	% error	2.52	1.72	0.80
0.04	Bottom wall	0.398	0.369	0.399
	Side wall	0.298	0.276	0.301
	Top wall	0.095	0.100	0.102
	% error	3.54	1.90	1.00
0.004	Bottom wall	0.379	0.340	0.360
	Side wall	0.274	0.248	0.263
	Top wall	0.099	0.098	0.099
	% error	1.63	1.76	0.56

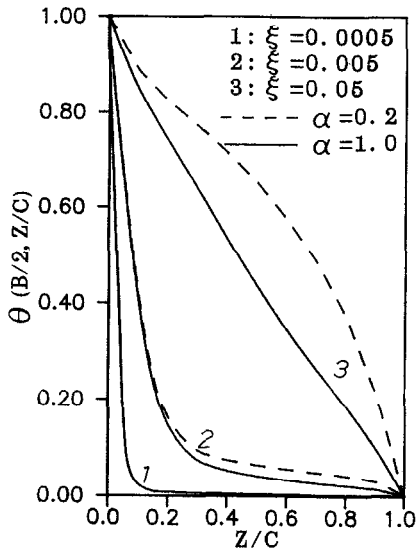

FIG. 2. Transient temperature distributions at the symmetry plane of a square medium ($\alpha = 1.0$) and a rectangular medium ($\alpha = 0.2$) with $N = 0.04$ and $C = 1.0$.

2% by 11×11-point scheme and within 1% by 21×21-point scheme. Besides, the results obtained by the two schemes are in good agreement for various N and $B = C$, as shown in Tables 2, 3 and 4. Hence it may be concluded that the 11×11-point scheme can generate accurate enough results.

The transient temperature distributions at the symmetry plane $Y = B/2$ of a square medium ($\alpha = 1.0$) and a wide rectangular medium ($\alpha = 0.2$) are presented in Fig. 2. Since for the cases considered the optical thickness C is fixed, a smaller aspect ratio $\alpha = C/B$ corresponds to a larger width B. For a medium with a smaller α the loss of energy from the side surfaces at $Y = 0$ and B is less and so its temperature distributions appear higher. As seen from Fig. 2, the effect of aspect ratios increases with time. Figure 2 also shows that in the late part of the transient heating process a steeper temperature gradient is formed at the bottom of the wide rectangular medium ($\alpha = 0.2$) with a small N. The temperature distribution in the wide rectangular medium is qualitatively similar to that in a one-dimensional slab [15].

Three-dimensional sketches of the temperature at $\xi = 0.05$ for $\omega = 0.8$ and $\omega = 0.0$ are presented respectively in Figs. 3(a) and (b). The temperature around the center of a medium with strong scattering ($\omega = 0.8$) is lower than that of a medium without scattering ($\omega = 0.0$), because the strongly scattering medium absorbs less energy from the heating surface in the transient heating process. The variation of temperature around the corner at $Y = 0$ and $Z = 0$ in the strongly scattering medium in contrast with that of a medium without scattering is mild. This is due to the energy redistribution by scattering. Besides, a steeper temperature gradient is not formed at the bottom of the highly scattering square medium.

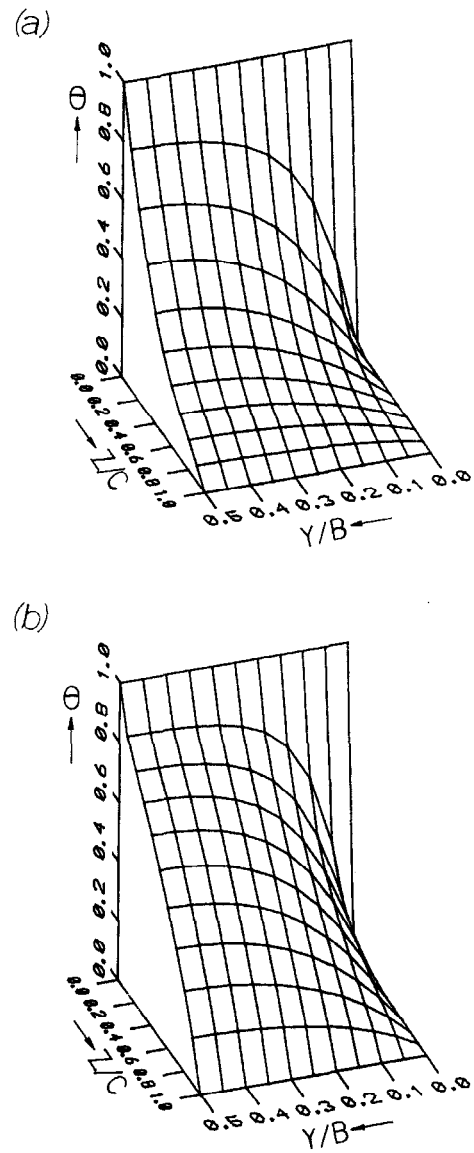

FIG. 3. Three-dimensional sketches of the temperature at $\xi = 0.05$ for media with $N = 0.04$ and $B = C = 1.0$. (a) $\omega = 0.8$, (b) $\omega = 0.0$.

Figures 4(a) and (b) show the effects of ω and N on the transient temperature distributions at the symmetry plane. The scattering albedo appears to have a small effect on the temperature distributions. Comparisons of Figs. 4(a) and (b) show that the decrease of N increases the dependence. For a fixed optical size and N, the temperature distributions at the symmetry plane in the heating process are usually higher for the case with a smaller ω, as shown in Figs. 3 and 4. As seen from Figs. 4(a) and (b), this tendency becomes apparent as time marches on.

The effects of the conduction-to-radiation parameter N on the total heat flux and the radiative heat flux are shown in Figs. 5(a) and (b), respectively. The dimensionless time ξ required to attain steady state increases as the value of N decreases. Moreover, keep-

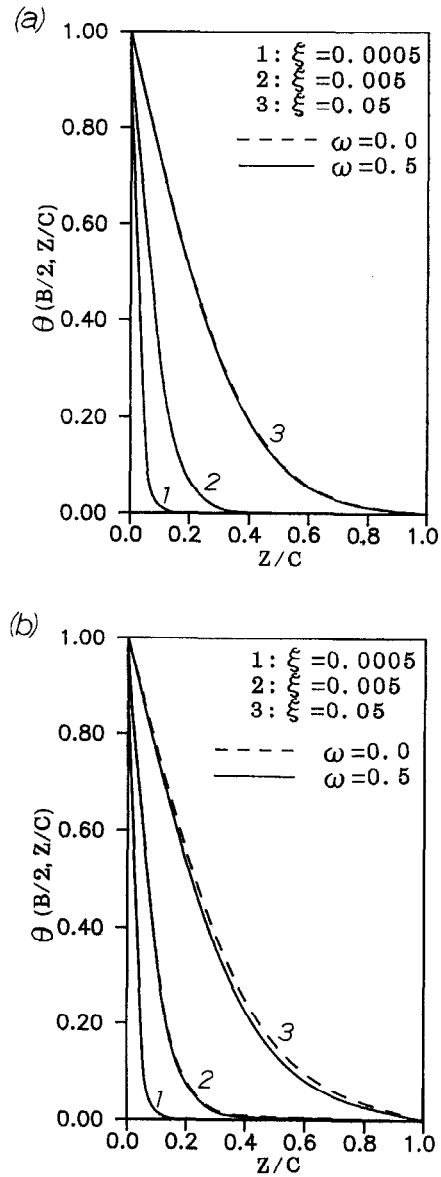

FIG. 4. Transient temperature distributions at the symmetry plane of a rectangular medium with $B = C = 1.0$. (a) $N = 4.0$, (b) $N = 0.4$.

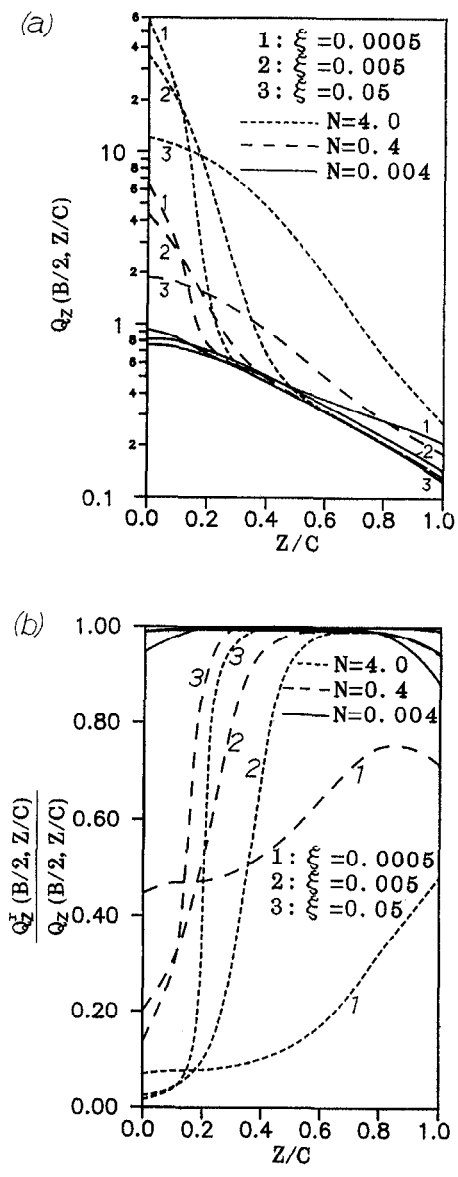

FIG. 5. Heat flux distributions at the symmetry plane of a square medium with $\omega = 0.5$ and $C = 1.0$ for a heating process. (a) Total heat flux, (b) ratio of radiative heat flux and total heat flux.

ing the medium size and the volumetric heat capacity fixed, the absolute time is inversely proportional to the thermal conductivity or the corresponding value of N for the cases considered. For example, we can interpret $\xi = 0.0005$ for $N = 0.4$ and $\xi = 0.005$ for $N = 4$ at the same absolute time. As seen from Fig. 5(a), at the same absolute time the heat flux in the vicinity of the hot wall is larger for the case of larger N. Figure 5(b) shows that, in general, the importance of radiative heat transfer becomes greater and radiative heat effects of the heating wall extend further into the medium as ξ increases. As the conduction-to-radiation parameter is lowered to a value of $N = 0.004$ the medium is radiation-dominated and the contribution of the conductive heat flux is almost negligible except in the vicinity of the walls. When the conduction-to-radiation parameter is increased to a value of $N = 0.4$, the medium near the hot wall is dominated by conduction. In the early part of the transient heating process, conduction is the dominant transfer mode for $N \geqslant 0.4$, as shown in Fig. 5(b).

Table 5 shows the heat flux at the center point of the bottom surface for $N = 4.0$ and 0.04. The discrepancies between the results obtained by the MDA with $\Delta Y = \Delta Z = 1/20$ and $1/24$ are less than 7×10^{-3} for all the cases considered. Thus, $\Delta Y = \Delta Z = 1/24$ is assumed to be small enough for the present problem. Comparisons of the results obtained by the MDA and those obtained by the ordinary P-3 approximation [3]

Table 5. Comparative results of $Q_z(B/20)$ for rectangular media with $C = 1.0$, $\theta_1 = 1.0$, $\theta_2 = 0.5$ and various aspect ratios

N	α	P-1 [3]	P-3 [3]	MDA ($\Delta Y = \Delta Z = 1/20$)	MDA ($\Delta Y = \Delta Z = 1/24$)	Integral [5]
4.0	0.5	9.852	9.048	9.030	8.969	8.772
	1.0	5.203	4.877	4.863	4.860	4.701
	2.0	3.155	3.032	3.087	3.086	
	5.0	2.640	2.592	2.619	2.619	
0.04	0.5	1.263	1.027	0.944	0.948	0.871
	1.0	1.019	0.817	0.693	0.694	0.780
	2.0	0.779	0.664	0.693	0.695	
	5.0	0.625	0.584	0.590	0.591	

show good agreement. Further comparisons to the solution of the integral equation show that the results obtained by both approximations are close to those obtained by solving the exact integral formulation numerically. In general, the accuracy of the MDA is superior to that of the P-1 approximation and almost equivalent to that of the P-3 approximation, as shown in Table 5. For more discussions about the differential approximations for radiative transfer, a number of references [3, 12–14 and 17–18] are available.

Acknowledgement—This work was supported by the National Science Council of the Republic of China in Taiwan through Grant NSC 80-0401-E006-34.

REFERENCES

1. R. Viskanta, Radiation heat transfer: interaction with conduction and convection and approximate methods in radiation, *Proceedings of the Seventh International Heat Transfer Conference*, Vol. 1, pp. 103–121. Hemisphere, Washington, DC (1982).
2. R. Siegel and J. R. Howell, *Thermal Radiation Heat Transfer* (3rd Edn), Chap. 16. Hemisphere, Washington, DC (1992).
3. A. C. Ratzel and J. R. Howell, Two-dimensional energy transfer in radiatively participating media with conduction by the P-N approximation, *Proceedings of the Seventh International Heat Transfer Conference*, Vol. 2, pp. 535–540. Hemisphere, Washington, DC (1982).
4. M. M. Razzaque, J. R. Howell and D. E. Klein, Coupled radiative and conductive heat transfer in a two-dimensional rectangular enclosure with gray participating media using finite elements, *J. Heat Transfer* **106,** 613–619 (1984).
5. W. W. Yuen and E. E. Takara, Analysis of combined conductive-radiative heat transfer in a two-dimensional rectangular enclosure with a grey medium, *J. Heat Transfer* **110,** 468–474 (1988).
6. M. E. Larsen and J. R. Howell, The exchange factor method: an alternative basis for zonal analysis of radiating enclosures, *J. Heat Transfer* **107,** 936–942 (1985).
7. C.-H. Ho and M. N. Özisik, Combined conduction and radiation in a two-dimensional rectangular enclosure, *Numer. Heat Transfer* **13,** 229–239 (1988).
8. T. Y. Kim and S. W. Baek, Analysis of combined conductive and radiative heat transfer in a two-dimensional rectangular enclosure using the discrete ordinates method, *Int. J. Heat Mass Transfer* **34,** 2265–2273 (1991).
9. D. W. Amlin and S. A. Korpela, Influence of thermal radiation on the temperature distribution in a semitransparent solid, *J. Heat Transfer* **101,** 76–80 (1979).
10. G. V. Derevyanko and P. S. Koltun, Radial-conductive heat transfer of semitransparent bodies, *J. Engng Phys.* **61,** 680–684 (1991).
11. A. L. Crosbie and R. G. Schrenker, Radiative transfer in a two-dimensional rectangular medium exposed to diffuse radiation, *J. Quant. Spectrosc. Radiat. Transfer* **31,** 339–372 (1984).
12. D. B. Olfe, A modification of the differential approximation for radiative transfer, *AIAA J.* **5,** 638–643 (1967).
13. C.-Y. Wu, W. H. Sutton and T. J. Love, Successive improvement of the modified differential approximation in radiative heat transfer, *J. Thermophys.* **1,** 296–300 (1987).
14. M. F. Modest, The modified differential approximation for radiative transfer in general three-dimensional media, *J. Thermophys.* **3,** 283–288 (1989).
15. C. C. Lii and M. N. Özisik, Transient radiation and conduction in an absorbing, emitting, scattering slab with reflective boundaries, *Int. J. Heat Mass Transfer* **15,** 1175–1179 (1972).
16. W. H. Sutton, A short time solution for coupled conduction and radiation in a participating slab geometry, *J. Heat Transfer* **108,** 465–466 (1984).
17. P. Cheng, Exact solutions and differential approximation for multi-dimensional radiative transfer in Cartesian coordinate configurations, *Progress in Astronautics and Aeronautics*, Vol. 31, pp. 269–308. AIAA, New York (1973).
18. F. H. Azad and M. F. Modest, Evaluation of the radiative heat flux in absorbing, emitting and linear-anisotropically scattering cylindrical media, *J. Heat Transfer* **103,** 350–356 (1981).